J Mater Sci (2017) 52:13040–13053

Chemical routes to materials

Characterizing the feasibility of processing wet granular materials to improve rheology for 3D printing

Michael Sweeney[1], Loudon L. Campbell[1], Jeff Hanson[1], Michelle L. Pantoya[1], and Gordon F. Christopher[1,*]

[1] *Mechanical Engineering Department, Texas Tech University, Lubbock, TX 79424, USA*

Received: 7 June 2017
Accepted: 17 July 2017
Published online: 26 July 2017

ABSTRACT

Rheological measurements and extrusion tests are used to evaluate the viability of high mass fraction (80% solids content) wet granular materials for extrusion-based 3D printing. Such materials have diverse applications from making dense, strong ceramic custom parts to 3D printing uniquely shaped energetic materials. Traditionally, 3D-printed colloidal materials use much lower mass fraction inks, and hence, those technologies will not work for systems requiring higher mass fraction solids content. These wet granular materials are highly non-Newtonian presenting non-homogenous flows, shear thinning, yield stress, and high elasticity. Such behaviors improve some aspects of print quality, but make printing very difficult. In this work, the relationship between the rheological behavior of wet granular materials and the processing parameters that are necessary for successfully extruding these materials for printing is examined. In the future, such characterizations will provide key indicators on how to alter printer design/operating conditions and adjust material behavior in order to improve printability. This study is a fundamental first step to successfully developing 3D printing technology of wet granular materials.

Introduction

Additive (i.e., 3D) printing technologies have immense potential to impact a wide range of industrial, scientific, and medical applications due to their ability to reduce material usage, decrease manufacture costs, enable on-demand production, and fabricate unique shapes. The major research thrusts in this area have been the development of new tools and techniques that will allow the use of a wider range of polymers, biomaterials, ceramics, and metals [1–5]. In particular, colloidal materials have been a major interest [6–13], because through variation of the type of colloid and solvent/binder system, fabrication of ceramics [9, 12–19], conductive pastes [20, 21], and medical materials [3, 9] is possible. However, 3D printing of colloidal materials has been limited to volume fractions of approximately 60% or less [6], and such prints often require post-processing to create final products with desired colloid mass fraction, void fraction, or surface properties [22]. Characterizing higher mass fraction colloids helps fill this gap toward processing a wider range of materials using additive manufacturing strategies.

Address correspondence to E-mail: gordon.christopher@ttu.edu

DOI 10.1007/s10853-017-1404-z

One advantage to processing higher colloidal mass fractions is that the final product will be denser with less void space, allowing mechanically stronger materials with less need for post-processing. This issue is important in creating stronger ceramic materials and also 3D printing energetic materials. Energetic composites are typically at least 75 wt% energetic components with the remaining binder required to hold the formulation together. The energetic components could include fuel particles such as aluminum (Al) or boron (B) combined with organic explosives such as PETN, TNT, RDX, or HMX and may also include propellants such as ammonium perchlorate (AP) [23]. Energetic composites are typically casted or molded, which can be time-consuming, expensive, wasteful, and difficult to adapt to new designs. But 3D printing can create more complex, unique geometries on demand, facilitating fast optimization of performance for mission-specific criteria that cannot be attained using traditional processing. Overall, 3D printing of energetics would reduce the need for excessive handling, post-processing, and stockpiling, conferring benefits to safety, cost, waste, and flexibility. For these reasons, advanced manufacturing of energetic composites is an important goal [23–29]. However, any energetic formulation designed for printing would need much higher mass fractions to create a viable material and avoid post-processing, thus the need for research on processing wet granular materials with solids loadings of at least 80 wt%.

Such high mass fraction colloidal formulations are best described as wet granular materials, where solvent and/or binder does not fully penetrate the entire void space between particles. The combination of both "hard" collisional-based interactions and "soft" viscous and surface tension-based interactions between particles creates a material that has a complex, non-Newtonian response to deformation. Such materials exhibit a range of unique challenges in their response to deformation that may make their utilization in 3D printing techniques particularly difficult. The goal of this paper is to explore the feasibility of extrusion-based 3D printing of wet granular materials by characterizing the rheology of a model material as well as its behavior under extrusion similar to what would be found in actual 3D printing technologies.

Background

Rheology effects on printability and print quality

Many printing materials exhibit non-Newtonian, viscoplastic, or viscoelastic behaviors such as shear thinning, yielding, or shear thickening. The ability and quality of any additive manufacturing processes such as 3D printing are very dependent on material rheology in terms of both printability and print quality. Unfortunately, the necessary properties that result in good final print quality are often at odds with those that make for easy printing, requiring a delicate optimization [6, 7].

The process of extrusion-based printing is always easier for materials with low yield stresses and viscosity. This is due to the effect of these parameters on the minimum pressure to create flow and the sustained pressure drop needed to drive flow through the nozzle. The minimum pressure needed to create flow for a material with a yield stress in a circular tube is described by Eq. (1) [30].

$$P_{\min} = \left(\frac{4L}{D}\right)\tau_{\text{yield}} \tag{1}$$

In Eq. (1), $P_{\min}$ is the minimum driving pressure, L is the length of the extrusion nozzle, D is the diameter of the nozzle, and τ_{yield} is the material yield stress. As can be seen in Eq. (1), lower yield stress values reduce minimum driving pressure [8, 9, 15, 30]. This is desirable in 3D printing, since the flow is not continuous but frequently starts and stops during a print. High yield stresses will require the machine to constantly apply large pressures to overcome yield, which will require a more robust system capable of constantly and reliably applying such pressures in a controlled manner.

After yield, the continuous driving pressure necessary for a given flow rate in a circular tube will depend on desired flow rate and viscosity. A basic non-Newtonian model is a power law fluid,

$$\mu_{\text{eff}} = k\dot{\gamma}^{n-1} \tag{2}$$

where μ_{eff} is the effective viscosity at a particular shear rate, $\dot{\gamma}$ is shear rate, k is the consistency index, and n is the power law exponent that determines the degree of shear thinning or thickening. Newtonian fluids have $n = 1$. For $n < 1$, fluids shear thin with smaller values of n indicating more significant shear

thinning. For $n > 1$, materials shear thicken. Although this model is simplistic and only captures shear behavior, it allows us to understand in a simple way how these behaviors will affect the flow in a nozzle in terms of the relationship between flow rate and pressure [31],

$$Q = \frac{\pi R^3}{\frac{1}{n}+3}\left(\frac{\Delta P}{L}\frac{R}{2k}\right)^{\frac{1}{n}} \quad (3)$$

In Eq. (3), Q is the volumetric flow rate, r is tube radius, ΔP is pressure drop, and L is tube length. As can be seen, lower consistency indices (k) will result in a lower pressure requirement for higher flow rates, and smaller n will create materials that are easier to flow as applied pressure increases. In general, to reduce continuous driving pressure for a desired flow rate, low k and n are advantageous [8, 9, 15, 30].

Printability is also affected by how an extruded material exits a nozzle of a printer. Viscoelastic materials forming threads are prone to a wide array of unhelpful behaviors, in particular jet breakup and satellite drop formation. Jet breakup due to capillary forces is a natural phenomenon that would make sustained printing difficult. Elasticity tends to stabilize jets against breakup, which is advantageous. However, it also means stopping printing quickly is more difficult since elastic fluids will be more stable. Alternately, shear thinning can accelerate breakup, which would be problematic if breakup occurs before printing is finished. Furthermore, high elasticity materials with long relaxation times can exhibit the formation satellite drops or beads on a string phenomenon during breakup, which would also be problematic to printing. Obviously, any of these phenomena would negatively impact the ability of a material to be printed continuously with controlled diameter. In general then, if materials have high relaxation times and elasticity without yield, breakup and satellite drop formation may be a concern. Yielding fluids will avoid some of these issues, but are prone to snap off behavior at critical thread dimensions, which could also affect continuous printing [32–35].

Print quality is the ability of the printed material to match the intended design, stay in place once printed, and maintain its printed shape. However, many printability problems bleed into print quality. For instance, material viscosity will also affect print fidelity and processing times by limiting the rate at which the print head can move, since mismatch between printed heads and extrusion rate can cause changes to extruded filament diameter. Therefore, shear thinning can create resolution difficulties if the pressure in the extrusion nozzle is not well controlled [7–9, 15, 30]. Thread breakup will affect the ability of the printer to match the programmed design and may cause significant deviations in design. Other problems that may occur at the nozzle include die swell [36, 37], in which an extruded viscoelastic material expands immediately at the tip of a nozzle due to large normal stresses; this would affect print resolution. In general, filament breakup and die swell are related to the overall elasticity of extruded materials; larger storage moduli and relaxation times would cause more complicated filament breakup behaviors and greater die swell in general.

Print quality is generally improved by printed materials being able to support their own weight and avoid road spread, the widening of the printed thread due to gravity. High yield stress is a benefit in avoiding this issue, since a material with a yield stress will not flow under quiescent conditions, avoiding road spread. Shear thinning is also beneficial, since such materials will be more resistant to flow under quiescent conditions as well. In general, elastic materials better maintain their shape and recover the initial shape after stress relaxation from the printing process [7–9, 15, 30]. Print quality is most benefited by larger yield stresses and elasticity; however, these properties typically increase the necessary driving pressure and can also create instabilities which can both stop printing and/or affect surface properties of the material.

Wet granular materials for 3D printing

In broad perspective, 3D-printed colloidal materials can be categorized in three ways: (1) low volume concentration suspensions of non-attractive particles; (2) low to higher concentration of attractive particles that form colloidal gels, and (3) higher concentrations of repulsive particles that can form colloidal glasses. All of these materials are non-Newtonian in shear, and depending on the specific composition they can exhibit shear thinning, shear thickening, yield stress, and other viscoelastic or viscoplastic behaviors. The mechanisms and range of these behaviors have been widely documented and studied in other literature [38–40]. Above the volume

fractions typically used in the majority of 3D printing of colloidal materials (~60%), the volume fraction of particles becomes so large that the liquid does not fully occupy the void space.

These materials are classified as "wet granular" materials, in which particles are the primary component and liquid bridges gaps between particles. The magnitude of the soft cohesion forces caused by capillary bridges is affected by individual particle dimensions, liquid volume, and formation/breakup, creating a hysteretic and statistic nature to the cohesion. Due to the combination of hard and soft interactions this creates, wet granular materials exhibit several regimes of flow behavior, which are characterized through the use of the non-dimensional inertial number (I) defined by Eq. (3) [41]. In Eq. (3), ρ is the average density of the composite and all other terms have been previously defined.

$$I = \frac{\dot{\gamma} d}{\sqrt{P/\rho}} \tag{4}$$

Initially, stresses are not large enough to breakup local particle jamming, and there is no flow [41]. Yield stress will depend on the confining pressure applied as well as the magnitude of friction and cohesion interactions [42, 43]. After yielding, wet granular systems typically present non-homogenous flow response to deformation due to local jamming, capillary force behavior, and the statistic nature of the collisions. Because of this, the local shear stress can be independent of global shear rates [44–46]. Simple continuous shear is rarely seen in such systems, instead local areas of low mass fraction particles will typically shear first due to their less restricted movement [47], which often occurs near the boundaries of the material [48].

For $I \ll 1$, flow is in a quasi-static regime where particle friction and cohesion forces dominate flow response. Particle movement is restricted by the size of local aggregates, frictional contact, and the magnitude of the cohesive interactions. The size of jammed clusters will decrease with increasing I, allowing greater movement and reduced resistance to deformation [49–51]. It is possible in the quasi-static regime to have regions of non-yielded material flow by being carried by bands of yielded materials [52], creating sliding layers of particles [53] that can also show stick–slip behavior [54].

For $I \gg 1$, particles become fluidized and resistance is collision based. Non-homogenous behavior will present itself as shear banding in the intermediate and collisional regimes [45–48, 50, 55]. The size and nature of the bands are directly related to the amount of solvent in such systems, with increasing larger bands with increasing solvent content and variation in solvent viscosity [46, 55]. Streamline curvature will generally also result in increased shear banding due to particle migration caused by curvature in the streamlines [45]. Intermediate regimes occur at $I \sim 1$, where particles are somewhat mobilized to flow, but still subject to friction and cohesion forces.

Because of the above behaviors, rheological measurement of such materials is quite difficult and is still a major challenge [56]. In fact, the measurement technique and processing method will often determine the value of such materials measured, indicating that it is difficult to some degree to translate rheology results to other processes [43, 44, 49]. Furthermore, the rheology of wet granular materials is unsurprisingly very system specific, but does tend to exhibit a range of common behaviors.

Typically, wet granular materials will exhibit some degree of shear thinning, with viscosity decreasing with increasing shear rate or inertia number [55, 57]. These flows can often be modeled as power law fluids or Herschel–Bulkley in these regimes [57].

The overall magnitude of the viscosity will vary greatly as particle properties and solvent are changed. Increasing particle roughness typically increases overall dissipation due to increased friction and also changes in the structure of capillary bridges [46]. Particle size will also affect overall viscosity. Increasing particle size creates less viscous material by decreasing the effect of the viscosity and capillary bridge and creating more deformable clusters of particles [54, 58]. Larger particles will also often exhibit lower yield [54]. Bimodal distributions of particles will also tend to decrease viscosity. Changes to particle surface chemistry can result in changes to solvent wettability. Increasing wettability tends to make systems more viscous and elastic due to increased strength of capillary bridges and large granule size [59, 60].

Materials and methods

Material preparation

An inert formulation was designed for this study to avoid the influences of reactivity and focus on the

rheological characteristics of processing a mock energetic mixture. The formulation is composed of a rough, polydisperse colloidal powder that is representative of the metallic colloids found in energetic composites. The colloidal particles are pentaerythritol (PET) and are millimeter-sized particles obtained from Alfa-Aesar. For energetic material combustion, a particle diameter that is 100 microns or smaller is ideal for fastest burn times [61]. To create the representative energetic mixture, the powder particle size was reduced with a Retsch CryoMill using a frequency of 18 Hz for 30 s for a 5-g sample size. The sample is then placed in a Retsch AS 200 Basic sieve shaker for 60 min at a frequency ranging from 2 to 3 Hz. This is done through several different sieve sizes to create several representative particle size ranges: 38–75 microns, 75–90 microns, and 250–350 microns. The distribution of diameters has not been characterized for this study. In typical energetic formulations, there would be a wide distribution of particle diameters as in this mock mixture. Figure 1 show scanning electron microscope (SEM) images of the powder post-milling.

To complete the system, a silicone-based binder (PDMS) was obtained from Dow Corning (Sylgard 182); this material is added without curing agent. The final mass fraction of all tested systems was 80% by mass solids and 20% by mass PDMS. When preparing the mixture, the colloids were mixed with silicone binder using a THINKY ARE-310 planetary centrifugal mixer at 2000 RPM for 2 min and 2200 RPM for 30 s in the opposite direction to defoam the mixture and eliminate air bubbles. Figure 2 shows photographs of the materials used in Table 1. In general, as particle size decreases, the mixtures resemble more cohesive materials. For the smallest particle system, the final material represents a silly putty-like material (Fig. 2b). As size increases, the material looks more like wet sand (Fig. 2d); finally, at the largest particle size (Fig. 2f), the mixture is very course and loosely held together.

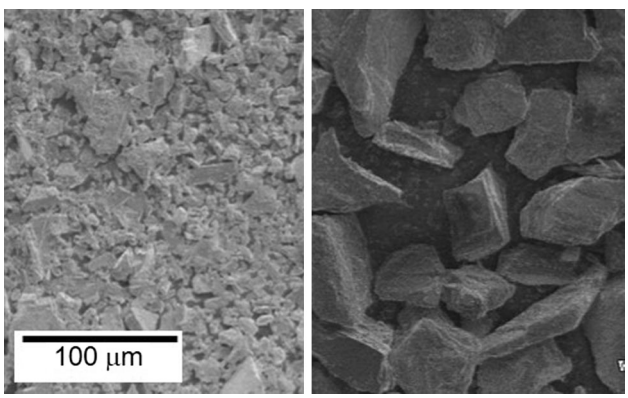

Figure 1 SEM images of (*left*) particles recovered from 38 to 75-micron sieves and (*right*) particles recovered from 75 to 90-micron sieves.

Rheology

To characterize the rheological properties of the mixture, a TA Instruments Discovery HR-3 rheometer was used with a 20-mm parallel plate geometry and a Peltier plate set to 25 °C. The sample was placed between the parallel plate and Peltier plate at a gap set to 1000 microns. Using the system in both steady shear and oscillatory shear allows characterization of viscosity and elastic and viscous moduli. Furthermore, normal pressure is recorded during tests, which can be used in the calculation of I (see Eq. 3).

As noted above, the non-homogenous shear response of these materials is well established. There are no means to visualize these flows during tests, so there is no way to ascertain whether shear banding or plug-like flows occur. Hence, all reported viscosities and moduli should be considered apparent values based on the assumption of a typical Couette flow field as would be created by a parallel plate geometry used here. A concern with these materials is fracture. This can typically be observed during experiments on the edge of the material visible under the parallel plate. No evidence of fracture throughout experimentation is observed by visually inspecting the edge of the materials.

Results and discussion

Printability

In order to gauge printability of wet granular solids, their behavior under steady shear at a range of shear rates is examined. Using the three ranges of powder sizes at 80% solids loading by mass, viscosity was measured over a range of shear rates as shown in Fig. 3. The first thing to note is that for all particle sizes, the materials are non-Newtonian with pronounced shear thinning across all shear rates. As particle size decreases, overall viscosity magnitude

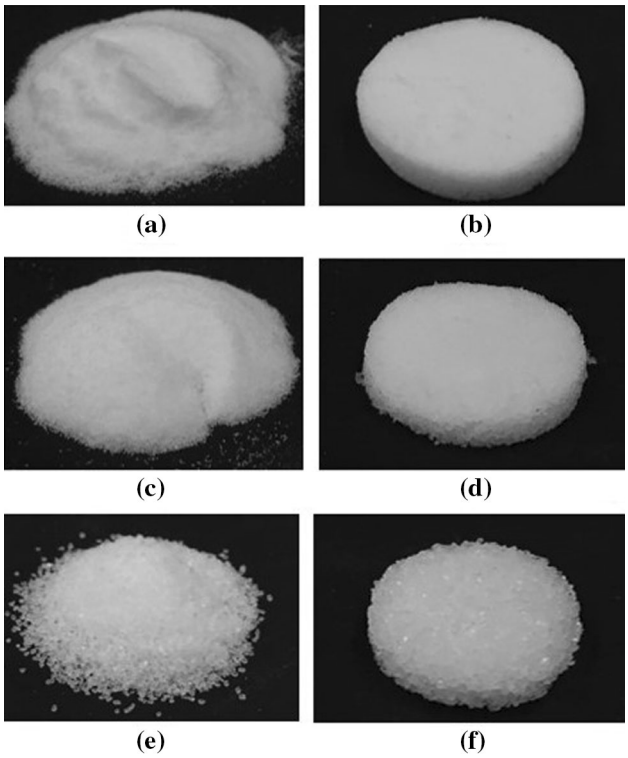

Figure 2 **a** 38 to 75-μm particles without any binder and **b** same particles 80% by weight with 20% PDMS. **c** 75 to 90-μm particles without any binder and **d** same particles 80% by weight with 20% PDMS. **e** 250 to 350-μm particles without any binder and **f** same particles 80% by weight with 20% PDMS.

Table 1 Results of fit of power law model to quasi-static flow regimes

Particle size (μm)	K	n
38–75	2502	−0.14
75–90	948	0.075
250–350	308	0.13

increases at all shear rates, which can be attributed to the larger surface area of the smaller particle size groups creating more inter-particle friction and hence resistance to flow. Also, liquid bridges in this system will have smaller radii and hence larger Laplace pressures and surface tension forces, which will also increase viscosity. The degree of shear thinning in all sample materials is approximately similar despite the difference in viscosity magnitudes. However, at the lowest shear rates tested, the viscosity begins to diverge for the smaller two particle distributions, indicating these materials definitely have a finite yield stress. The materials all have a distinctive transition in the degree of shear thinning that occurs at a shear rate between 1 and 10 s^{-1}, which may indicate a transition to the collisional regime.

The viscosity data are replotted as a function of inertial number (Eq. 3) using the density of the materials as calculated by their combined mass fractions and normal stress data from the rheometer, in Fig. 3b. At low I in the quasi-static to transitional regimes, there is a clear dependence on particle size, where friction would be important. The previously seen transition in behavior now occurs at an inertial number of ~100. After this point, the data collapse onto a single line for all particle sizes. This indicates a transition to the collisional regime where the inter-particle collisions determine rheology rather than friction and surface tension forces. The reduced dependence on particle size is due to the reduction in these two forces that are dominated by particle size. Although particle size does affect likelihood of collision between particles, it would appear mass fraction is the more important controller of this behavior. Since all systems shown in Fig. 3 are at identical mass fractions, the viscosity curves collapse into a single trend for $I > 100$.

The nature of the observed shear thinning in the quasi-static regime is further explored by attempting to fit the data to the simple power law model from Eq. (2). Table 1 shows the results of the fit to all data before the change in slope between at 1 s^{-1} (i.e., before the material is in the collisional regime). All fits in this range of data had $R^2 > 0.99$. As Table 1 shows, the shear thinning exponents are exceptionally small, and in fact negative for the smallest particles. Shear thinning exponents approaching or less than 0 indicate a yielding, since for a yielding material, stress will be proportional to inverse of shear rate [62]; therefore, it is concluded that the smallest two materials indeed have a yield stress and are deforming in the quasi-static regime. Hence, the local behavior of this material will be very different than the average global data recorded by the rheometer. The largest particle data show significant shear thinning, but with a very small, although nonzero exponent. It is possible that this material either has a very small yield stress which is not being captured by the rheometer, or perhaps does not have a yield stress. In either case, the material also would be considered to be in the quasi-static flow regime, but shows a truer shear thinning-like behavior. For all materials, being in the quasi-static to transitional

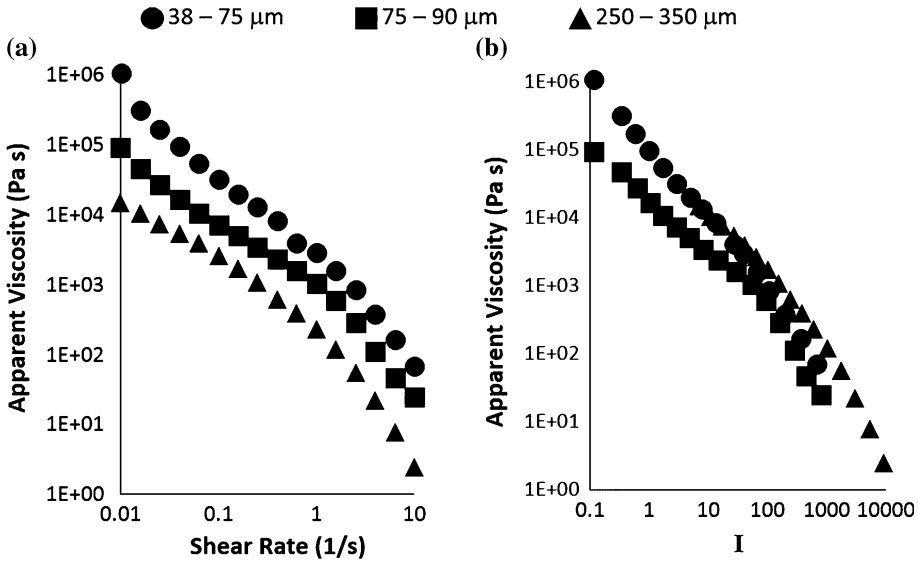

Figure 3 **a** Viscosity data for all particle sizes compositions at 80% by weight solids and 20% PDMS as a function of shear rate. **b** Identical data to **a** but plotted versus inertial number using normal force data obtained from rheometer.

regimes would also indicate a high dependence on particle friction, which is why the pronounced dependence on particle size is observed. The high values of k indicate the overall large resistance to flow this materials have, which decreases with increasing particle size. When the data in the collisional regime are fitted to the power law fluid model of Eq. (2), all materials have $n < 0$, indicating all materials have yielded, as expected.

The data in general indicate that these materials have very high viscosity and will make printing difficult, especially for smaller particles. The high viscosities at low shear rates indicate tremendous pressures will be needed in order to create flow. However, at higher I or shear rates, transition to collisional flows alleviates this problem since all materials exhibit significant shear thinning. In general, printing smaller particle mixes may be possible provided shear rates are high enough. However, the overall larger viscosities of smaller particle systems will likely reduce extrusion rates which will reduce print head speed. In general, the materials present the possibility to be presented but will likely have a restrictive operational phase space within which printing will be possible.

Looking at the viscosity results in Fig. 3, the major concern for printability is the high viscosity that make printing very difficult due to high driving pressures required. One way to deal with such a condition is to apply a pre-shear to the material before printing. Pre-shearing/conditioning applies a known flow to a material to modify its state in order to create lower initial viscosities. In this case, pre-shear could rearrange particles out of the jammed state and into a more collisional mode before actual printing begins.

Figure 4a shows the effectiveness of pre-shear based on time of applied pre-shear. A 2 s^{-1} shear was applied for varying durations, and viscosity is reduced by an order of magnitude as pre-shear time varies from 0 to 10 min. The reduction in viscosity is attributed to particle rearrangement creating a less jammed state, allowing flow to occur in the transitional/collisional regime at I earlier than indicated in Fig. 3. The pre-shear time has a moderate effect on the viscosity reduction, which is most evident at the lowest shear rates tested. However, at higher I where transition to the collisional regime was seen in Fig. 3, all viscosity curves collapse onto a single trend. This indicates that a particle rearrangement at the applied pre-shear was not enough to move the microstructure fully into a collisional regime, and hence, all data collapse once that regime occurs.

In Fig. 4b, the effect of pre-shear magnitude is examined by applying two shear rates, one below the collisional regime and one above the collisional regime, to the system for 2 min and then examining the flow curve again. At the 2 s^{-1} shear rate, the same behavior is observed in Fig. 4a. However, the 10 s^{-1} shear rate behavior is very different; a low shear viscosity plateau is seen, and the high shear rate collisional regime does not collapse onto the previous

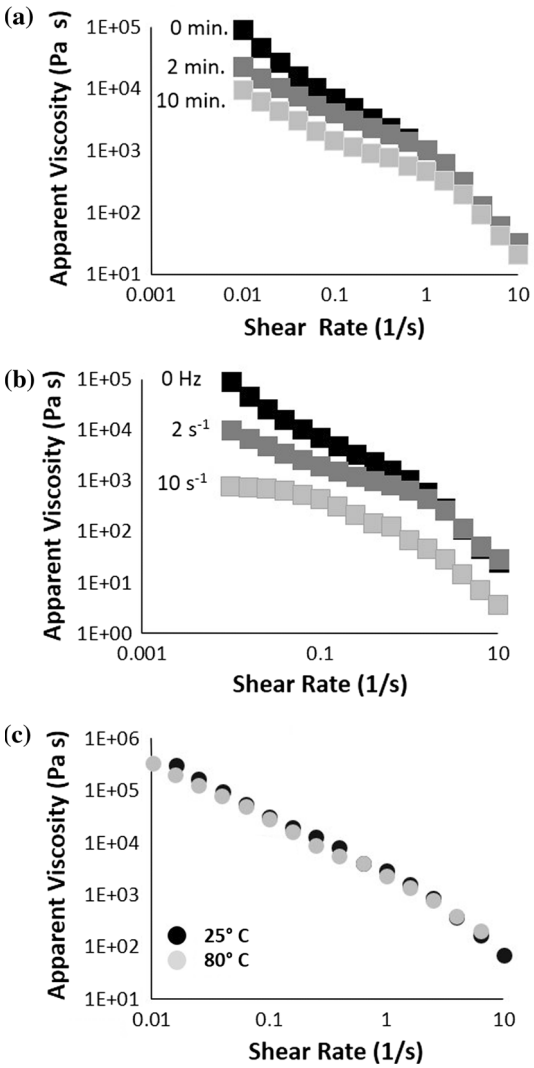

Figure 4 Effects of pre-shear on viscosity for 80% by weight 75–90-μm particle size with 20% PDMS. **a** Pre-shear of 2 s^{-1} was applied for 0, 2 and 10 min, and then, a shear rate sweep was immediately conducted. **b** Pre-shear is applied with 3 different shear rates for 2 min each, and then results of flow sweeps conducted immediately after are shown. **c** Effects of temperature on steady shear viscosity as a function of *I*.

collisional regime. Instead, the viscosity is always lower than the previous tests. At the lower pre-shear shear rate, the primary effect is the breakup of clusters, which allows material to flow more easily. However, the microstructure is still in the same basic state at the beginning of the flow curve. Above 10 s^{-1}, the material is already in the collisional regime, which means there is near-complete cluster breakup and particle migration due to shear. The microstructure is substantively different. Therefore, when the lower shear rates are immediately tested, the flow

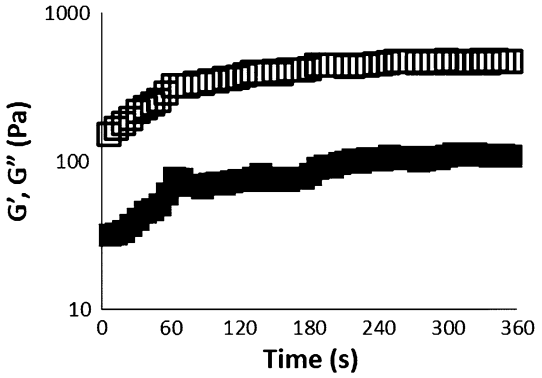

Figure 5 Recovery test for 80% by weight 75–90-μm particle size with 20% PDMS. Pre-shear was applied at 10 s^{-1} for 2 min and followed by a frequency sweep at 10 radians per second, 0.01% strain for 10 min.

response is completely modified, creating the zero shear viscosity plateau and lower overall viscosity at all shear rates.

One common means of reducing viscosity of any material is to heat it up rather than applying pre-shear (as shown in Fig. 4c). Although with energetic materials this may be unwise, Fig. 4c explores the concept in general as a means of increasing printability by reducing viscosity (Fig. 4c). Unsurprisingly, temperature does not have a large effect on these systems. This is because the particles are quite large and not in solution, so increased thermal motion/energy is not a major factor in their flow resistance, and because the binder (PDMS) is not known to be affected by temperature over this range [63]. Although this is particular to the system chosen for this study, other systems with more heat-sensitive binders may be better suited by such a technique.

For the effects shown in Fig. 4 to be useful, the wet granular material should maintain the pre-shear-induced properties for a substantial amount of time, allowing pre-shear of a material and then multiple print runs to maintain the new microstructure. It is important then to study how long the microstructure takes to revert back to its initial state after such flow is applied. To observe the timescales for how long the pre-shear conditions last, the same 10 s^{-1} pre-shear is applied to the material, and then, structure recovery is monitored with small amplitude oscillatory shear shown in Fig. 5. Recovery time is found to be approximately ~60 s. Figure 5 indicates that pre-shear is effective, but microstructure recovery is quite fast, and hence, any pauses in printing may negate the effects induced with pre-shear observed here.

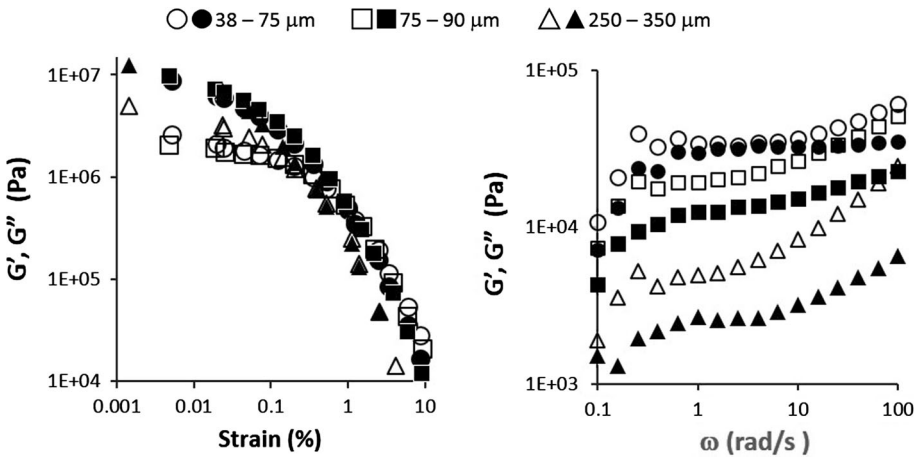

Figure 6 Small amplitude oscillatory shear data for mixes identical to those in Fig. 3. *Solid symbols* are for storage moduli, and *hollow* for loss moduli. (*Left*) Strain sweep (1 rad/s) and (*Right*) frequency sweep (1% strain).

Therefore, any thought of taking advantage of such behaviors will require significant planning of print head motion and starting/stopping during prints.

Print quality and extrusion

Final print quality is primarily determined by material viscoelasticity, yield stress, and relaxation time. Those values as a function of particle size are shown in Fig. 6. In general, all materials are viscoelastic with pronounced elasticity over a range of frequencies and strains. Looking at strain sweep data (Fig. 6a), all materials behave relatively similar, being primarily elastic over all strains. All the materials yield from the linear to nonlinear regime at an approximate a strain of 0.1%. Using this strain value and the storage moduli of the material, a yield stress for these materials can be estimated using the following relation, $\sigma_y = G'\gamma$, where G' and γ are taken from the yielding point on the strain sweep curves. For the values in Fig. 6a, the approximate yield stress is found to be 10 kPa. The linear regime is very small for these materials. After yield, all data collapse at large strains as materials move into transition/collision regime, similar to results in steady shear and pre-shear.

The frequency sweep data are in a regime in which the materials are slightly more viscous than elastic. There is moderate frequency dependence, but generally the moduli are consistent over the frequencies tested (Fig. 6a). The material should be in the quasi-static/jammed regime due to the low strains applied in this test, and so the response is expected to be similar to the initial points of the steady shear data. Indeed, similar particle dependence to steady shear tests is observed. From these data, it is observed that the crossover frequencies for these materials are likely occurring close to but below 0.1 rad/s, which means these materials should have a relaxation time of at least 60 s. This is in good agreement with the structural recovery experiments shown in Fig. 5. In general, the high yield and relaxation times are favorable for print stability of such materials.

Given the results from rheology analysis in Figs. 3, 4, 5, and 6, printability is characterized further by extruding the materials through a nozzle using a plunger driven by a high applied pressure (Fig. 7). Although wet granular materials are not typically used in 3D printing, they have been used in extrusion-based processes, particularly in the drug fabrication field where extrusion and spheronization are often used in the manufacturing of drug-loaded pellets [57, 64, 65]. Yield and elasticity make extrusion of such systems difficulty, and overall processes are quite dependent on rheology of a given material. Also, due to the high pressures required in such systems, there is often extrusion of the liquid phase from the solid mass, which can cause surface fracture and other problems. Overall, the extrusion of wet granular materials requires high pressures to overcome yield and large apparent viscosities and can be difficult to control final material properties due to weeping of wetting materials and non-local structure [30, 57, 64–66].

Given the rheology results, printing is expected to be difficult and require large pressures due to high viscosities and yield stress, especially without any significant pre-shear. Using Eq. (1) and the yield stress found above, the minimum pressures needed to drive flow in these tests are estimated. For the 3-mm nozzle, a P_{min} of 38 PSI and for the 1.6-mm

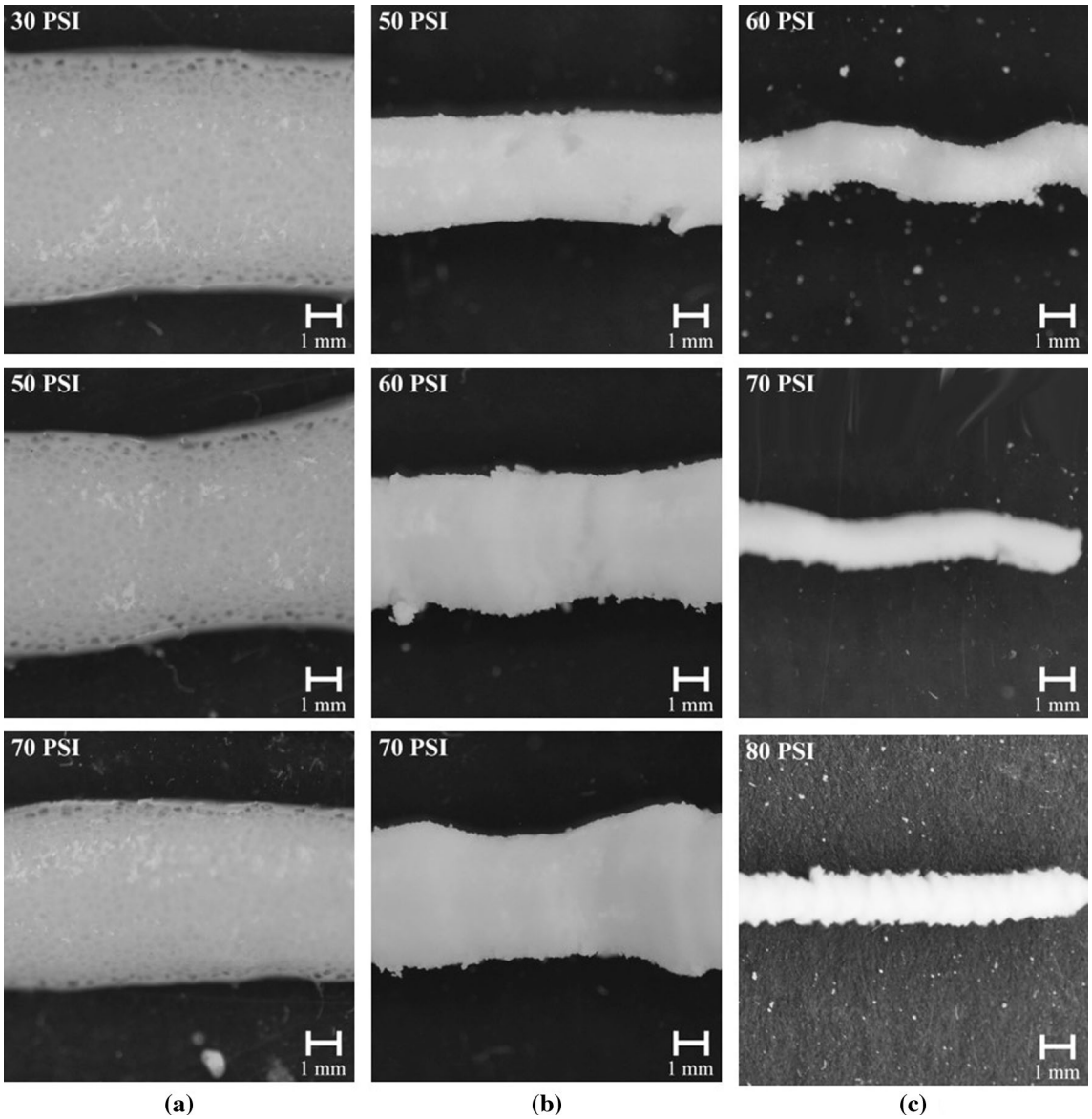

Figure 7 **a** 250–350-micron range extruded through 3-mm nozzle at varying pressures. **b** 38–75-micron range extruded through 3-mm nozzle at varying pressures. **c** 38–75-micron range extruded through 1.6-mm nozzle at varying pressures.

nozzle, a P_{min} of 72 PSI are calculated. These pressures are reasonably close to the minimum pressures used in Fig. 7, indicating the merit of rheological testing for such systems. They also indicate the relatively high pressures required to create flow, which as mentioned above can cause weeping and other issues.

It is difficult to estimate the extrusion speed of the materials using the power law model because for the first 2 fluids, the extremely low and/or negative exponents indicate its use is inaccurate. Also, it is difficult to gauge what flow regime the material is in, and whether the fitted data for the quasi-static regime is accurate. Although by using Eq. (3) and the values represented in Table 1, average velocities were estimates at 0.03–20 mm/s from the lowest to the largest applied pressure. We were not able to measure the speed of the fluid or the extrusion head using the current experimental setup, but believe these velocities are in line with what was observed. Without having an exact speed of the flow velocity, there was mismatch between the rate of extrusion and nozzle head print speed. Because of this, the final width of the extruded materials in Fig. 7 does not exactly

match nozzle diameter (3 mm for Fig. 7a, b and 1.6 mm for c). Although die swell could cause a similar effect, we believe the inconsistent nature of the width changes indicates this was primarily caused by the speed mismatch.

One difficulty in measuring the flow rate or the speed of the extrusion head in all tests was the significant issues in maintaining extrusion without snap off. Snap off is a typical mechanism of jet breakup in yield stress materials. There may be issues here in the print head speed and flow speed mismatch adding extra stresses which aided this behavior. However, in general snap off was worse with the increasingly smaller particles which showed more yield-like behavior.

Figure 7a displays results from the largest particle size mixture at a range of pressures through a 3-mm nozzle. All pressures give relatively consistent results in terms of ability to extrude. There is some variation in width of the materials, but overall width stays relatively consistent. This consistency is not affected by pressure. The final width of the extruded materials is slightly larger than the nozzle; this is due to variance between extrusion speed and movement of the nozzle. The particles are clearly visible in the extrusion, which should not be mistaken for air bubbles. This material was the least elastic and had the least yield-like behavior in all steady shear and oscillatory shear tests. No evidence of weeping is observed due to the high pressures applied; nor are there any visible issues due to the mix of high pressure and elasticity/yielding causing surface roughness, jet breakup or any other problem. The pressures needed here to create continuous flow were not used to estimate any flow rates with Eqs. (2, 3), given the inability to predict the transient flow regime.

Figure 7b displays the same nozzle but for a smaller particle size mix. The width is relatively consistent at all pressures. At higher applied pressures, there is more variation in the width. However, there are less defects at edges and surfaces at higher pressures. Furthermore, the maintaining of such dimensions indicates the high relaxation times and yield stress are inhibiting road spreading for these materials. The driving pressures all exceed the minimum calculated pressure based on estimated yield stress. There are no signs of surface roughness/fracture. As mentioned, these are typically high yield stress materials in spheronization. Given this material was indicating yield in steady shear tests, but was of significantly smaller overall viscosities in steady shear, it is not surprising to see some evidence of the high viscosity and yield on the surface properties.

The same material is printed through a smaller 1.6-mm nozzle in Fig. 7c. As pressure increases, surface defects are observed to increase due to high stress on material edges as extruded. Print widths, however, are much more consistent than all the other prints. Final diameters are slightly smaller than the nozzle, which again is due to large relaxation times and yield stresses inhibiting road spread. In general, material in this nozzle requires higher pressures to print. Good agreement between the minimum pressure required for extrusion and the estimated value from oscillatory shear is observed. This material had the most obvious yielding signature in steady shear, and unsurprisingly the greatest issues in surface quality are observed with these system. In particular, pronounced roughness all along the surface at the highest print pressure is seen. This indicates that the yield stress was causing significant deviations in ideal flow at the nozzle exit and neat snap off behavior was creating problems in the surface.

Conclusions

The feasibility of using higher mass fraction colloidal systems for 3D additive manufacturing through extrusion printing was studied through the use of rheology and some limited extrusion of such materials. Using a model material representative of many real energetic formulations and possible ceramic systems, there are some inherent difficulties in working with such materials in terms of both printability and print quality; however, through proper processing it may be possible to work with such materials. In particular, the high viscosity and yield stresses of these materials are problematic for successful printing using traditional pressure-only-based extrusion methods. Such high viscosities indicate the need for flow driven not just by pressure but also through a secondary mechanical means such as a positive displacement piston, auger, or some other mechanical system. These problems can be somewhat alleviated by creating shear rates large enough to create collisional flow regimes, which provide significant alteration of the microstructure of these systems to lower viscosity over a wide range of flow rates. Unfortunately, it also appears that any benefits of pre-shear may be short-lived.

Overall the materials have sufficient yield stress and elasticity to maintain its shape which bodes well for print quality. However, pronounced surface roughness at higher flow pressures for more elastic systems were seen, which is problematic. In general, these materials major issues appear to be on the printability side rather than print quality. The rheological profile of these materials creates significant challenges in print quality due to yield stress-induced surface roughness at high pressures as evidenced in extrusion tests.

These initial results indicate there is some promise in the potential of printing higher mass fraction colloidal materials. However, the phase space of possible processing speeds, flow rates, and resolutions will likely be severely limited in comparison with other lower mass fraction materials due to the non-trivial issues the complex rheology of these systems creates. Furthermore, there are still many larger questions that need to be explored in terms of the ability of layers to weld together during printing, resolutions, shear banding in nozzle, and curing times. Nonetheless, the potential of such materials to overcome flaws in lower mass fraction prints in terms of solids density and to open up new applications such an energetics printing warrants further study of such system beyond these initial feasibility tests.

Acknowledgements

The authors gratefully acknowledge support from the Army Research Office and DOE/Consolidated Nuclear Security, LLC-PANTEX.

References

[1] Schubert C, Van Langeveld MC, Donoso LA (2013) Innovations in 3D printing: a 3D overview from optics to organs. Br J Ophthalmol 98:159–161

[2] Rengier F, Mehndiratta A, von Tengg-Kobligk H, Zechmann CM, Unterhinninghofen R, Kauczor H-U, Giesel FL (2010) 3D printing based on imaging data: review of medical applications. Int J Comput Assist Radiol Surg 5(4):335–341

[3] Gross BC, Erkal JL, Lockwood SY, Chen C, Spence DM (2014) Evaluation of 3D printing and its potential impact on biotechnology and the chemical sciences. ACS Publications, Washington

[4] Vaezi M, Seitz H, Yang S (2013) A review on 3D micro-additive manufacturing technologies. Int J Adv Manuf Technol 67(5–8):1721–1754

[5] Shirazi SFS, Gharehkhani S, Mehrali M, Yarmand H, Metselaar HSC, Kadri NA, Osman NAA (2015) A review on powder-based additive manufacturing for tissue engineering: selective laser sintering and inkjet 3D printing. Sci Technol Adv Mater 16(3):033502

[6] Avery MP, Klein S, Richardson R, Bartlett P, Adams G, Dickin F, Simske S (2014) The rheology of dense colloidal pastes used in 3D-printing. In: NIP & Digital Fabrication Conference, vol 1. Society for Imaging Science and Technology, pp 140–145

[7] Conrad JC, Ferreira SR, Yoshikawa J, Shepherd RF, Ahn BY, Lewis JA (2011) Designing colloidal suspensions for directed materials assembly. Curr Opin Colloid Interface Sci 16(1):71–79. doi:10.1016/j.cocis.2010.11.002

[8] Lewis JA (2006) Direct ink writing of 3D functional materials. Adv Func Mater 16(17):2193–2204. doi:10.1002/adfm.200600434

[9] Lewis JA, Smay JE, Stuecker J, Cesarano J (2006) Direct ink writing of three-dimensional ceramic structures. J Am Ceram Soc 89(12):3599–3609. doi:10.1111/j.1551-2916.2006.01382.x

[10] Olhero SM, Ferreira JMF (2002) Particle segregation phenomena occurring during the slip casting process. Ceram Int 28(4):377–386. doi:10.1016/s0272-8842(01)00105-5

[11] Olhero SM, Ferreira JMF (2004) Influence of particle size distribution on rheology and particle packing of silica-based suspensions. Powder Technol 139(1):69–75. doi:10.1016/j.powtec.2003.10.004

[12] Philips NR, Compton BG, Begley MR (2012) High strength alumina micro-beams fabricated by inkjet printing. J Am Ceram Soc 95(10):3016–3018. doi:10.1111/j.1551-2916.2012.05395.x

[13] Schlordt T, Schwanke S, Keppner F, Fey T, Travitzky N, Greil P (2013) Robocasting of alumina hollow filament lattice structures. J Eur Ceram Soc 33(15–16):3243–3248. doi:10.1016/j.jeurceramsoc.2013.06.001

[14] Lu XS, Lee Y, Yang SF, Hao Y, Evans JRG, Parini CG (2010) Solvent-based paste extrusion solid freeforming. J Eur Ceram Soc 30(1):1–10. doi:10.1016/j.jeurceramsoc.2009.07.019

[15] Morissette SL, Lewis JA, Clem PG, Cesarano J, Dimos DB (2001) Direct-write fabrication of Pb (Nb, Zr, Ti) O_3 devices: influence of paste rheology on print morphology and component properties. J Am Ceram Soc 84(11):2462–2468

[16] Prasad P, Reddy AV, Rajesh PK, Ponnambalam P, Prakasan K (2006) Studies on rheology of ceramic inks and spread of ink droplets for direct ceramic ink jet printing. J Mater Process Technol 176(1–3):222–229. doi:10.1016/j.jmatprotec.2006.04.001

[17] Sakar-Deliormanli A, Celik E, Polat M (2008) Rheological behavior of PMN gels for solid freeform fabrication. Colloids Surf A Physicochem Eng Asp 324(1–3):159–166. doi:10.1016/j.colsurfa.2008.04.029

[18] Tari G, Ferreira JMF, Fonseca AT, Lyckfeldt O (1998) Influence of particle size distribution on colloidal processing of alumina. J Eur Ceram Soc 18(3):249–253. doi:10.1016/s0955-2219(97)00113-1

[19] Travitzky N, Bonet A, Dermeik B, Fey T, Filbert-Demut I, Schlier L, Schlordt T, Greil P (2014) Additive manufacturing of ceramic-based materials. Adv Eng Mater 16(6):729–754. doi:10.1002/adem.201400097

[20] Durairaj R, Ramesh S, Mallik S, Seman A, Ekere N (2009) Rheological characterisation and printing performance of Sn/Ag/Cu solder pastes. Mater Des 30(9):3812–3818. doi:10.1016/j.matdes.2009.01.028

[21] Nguyen HV, Andreassen E, Kristiansen H, Johannessen R, Hoivik N, Aasmundtveit KE (2013) Rheological characterization of a novel isotropic conductive adhesive—epoxy filled with metal-coated polymer spheres. Mater Des 46:784–793. doi:10.1016/j.matdes.2012.11.036

[22] Guillon O, Jamin C, Bordia RK (2010) Effect of drying conditions on patterned ceramic films processed by soft micromolding. J Ceram Soc Jpn 118(1376):321–325. doi:10.2109/jcersj2.118.321

[23] Fordham S (2013) High explosives and propellants. Elsevier, Amsterdam

[24] Sullivan KT, Zhu C, Duoss EB, Gash AE, Kolesky DB, Kuntz JD, Lewis JA, Spadaccini CM (2016) Controlling material reactivity using architecture. Adv Mater 28(10):1934–1939

[25] Borcherding R (1998) An alternative to open burning treatment of solid propellant manufacturing wastes. Waste Manage 17(2):135–141

[26] Clark B, Zhang Z, Christopher G, Pantoya ML (2017) 3D processing and characterization of acrylonitrile butadiene styrene (ABS) energetic thin films. J Mater Sci 52(2):993–1004. doi:10.1007/s10853-016-0395-5

[27] Meeks KA, Clark BR, Cano JE, Apblett CA, Pantoya ML (2015) Effects of rheological properties on reactivity of energetic thin films. Combust Flame 162(9):3288–3293

[28] Li X, Huang C, Yang H, Li Y, Cheng Y (2016) Thermal reaction properties of aluminum/copper (II) oxide/poly (vinylidene fluoride) nanocomposite. J Therm Anal Calorim 124(2):899–907

[29] Chiaverini MJ, Kuo KK, Lu FK (2007) Fundamentals of hybrid rocket combustion and propulsion. American Institute of Aeronautics and Astronautics, Reston, VA

[30] Pospischil M, Specht J, Konig M, Horteis M, Mohr C, Clement F, Biro D (2014) Paste rheology correlating with dispensed finger geometry. IEEE J Photovolt 4(1):498–503. doi:10.1109/jphotov.2013.2278657

[31] Beckstead M (2002) VKI special course internal aerodynamics in solid rocket propulsion. Rhode-Saint-Genese, Belgium

[32] McKinley GH (2005) Visco-elasto-capillary thinning and break-up of complex fluids, Rheol. Rev. 3, 1–48

[33] Rodd LE, Scott TP, Cooper-White JJ, McKinley GH (2004) Capillary break-up rheometry of low-viscosity elastic fluids. Appl Rheol 15(1):12–27

[34] Clasen C, Phillips PM, Palangetic L (2012) Dispensing of rheologically complex fluids: the map of misery. AIChE J 58(10):3242–3255

[35] Mathues W, McIlroy C, Harlen OG, Clasen C (2015) Capillary breakup of suspensions near pinch-off. Phys Fluids 27(9):093301

[36] Agarwal PK, Bagley EB, Hill CT (1978) Viscosity, modulus, and die swell of glass bead filled polystyrene-acrylonitrile copolymer. Polym Eng Sci 18(4):282–287

[37] Papanastasiou TC, Alexandrou A (1987) Isothermal extrusion of non-dilute fiber suspensions. J Nonnewton Fluid Mech 25(3):313–328

[38] Morris JF (2009) A review of microstructure in concentrated suspensions and its implications for rheology and bulk flow. Rheol Acta 48(8):909–923

[39] Van der Werff J, De Kruif C (1989) Hard-sphere colloidal dispersions: the scaling of rheological properties with particle size, volume fraction, and shear rate. J Rheol 33(3):421–454

[40] Mewis J, Wagner NJ (2012) Colloidal suspension rheology. Cambridge University Press, Cambridge

[41] Mills P, Rognon PG, Chevoir F (2008) Rheology and structure of granular materials near the jamming transition. EPL 81(6):3. doi:10.1209/0295-5075/81/64005

[42] Benarie M (1961) Rheology of granular material II-a method for the determination of the intergranular cohesion. Br J Appl Phys 12(9):514

[43] Cheng DCH, Kruszewski AP, Senior JR, Roberts TA (1990) The effect of particle-size distribution on the rheology of an industrial suspension. J Mater Sci 25(1A):353–373. doi:10.1007/bf00544230

[44] Daniel RC, Poloski AP, Saez AE (2008) Vane rheology of cohesionless glass beads. Powder Technol 181(3):237–248. doi:10.1016/j.powtec.2007.05.003

[45] de Cagny H, Fall A, Denn MM, Bonn D (2015) Local rheology of suspensions and dry granular materials. J Rheol 59(4):957–969. doi:10.1122/1.4919970

[46] Liao C-C, Hsiau S-S (2009) Influence of interstitial fluid viscosity on transport phenomenon in sheared granular materials. Chem Eng Sci 64(11):2562–2569

[47] Passman SL, Nunziato JW, Bailey PB, Reed KW (1986) Shearing motion of a fluid-saturated granular material. J Rheol 30(1):167–192

[48] Kuno H, Senna M (1967) Rheological behavior of powder in a rotational viscometer. Rheol Acta 6(3):284–288

[49] Poloski AP, Bredt PR, Daniel RC, Saez AE (2006) The contribution of frictional contacts to the shear strength of coarse glass bead powders and slurries. Rheol Acta 46(2):249–259. doi:10.1007/s00397-006-0105-3

[50] Rognon PG, Roux JN, Naaim M, Chevoir F (2008) Dense flows of cohesive granular materials. J Fluid Mech 596:21–47. doi:10.1017/s0022112007009329

[51] Williams PR, Williams DJ (1989) Rheometry for concentrated cohesive suspensions. J Coast Res 6(1):151–164

[52] Bouzid M, Trulsson M, Claudin P, Clement E, Andreotti B (2013) Nonlocal rheology of granular flows across yield conditions. Phys Rev Lett 111(23):154–155. doi:10.1103/PhysRevLett.111.238301

[53] Balendran B, Nematnasser S (1993) Viscoplastic flow of planar granular-materials. Mech Mater 16(1–2):1–12. doi:10.1016/0167-6636(93)90022-j

[54] Higashi N, Sumita I (2009) Experiments on granular rheology: effects of particle size and fluid viscosity. J Geophys Res Solid Earth. doi:10.1029/2008jb005999

[55] Schwarze R, Gladkyy A, Uhlig F, Luding S (2013) Rheology of weakly wetted granular materials: a comparison of experimental and numerical data. Granular Matter 15(4):455–465. doi:10.1007/s10035-013-0430-z

[56] Kawasaki T, Ikeda A, Berthier L (2014) Thinning or thickening? Multiple rheological regimes in dense suspensions of soft particles. EPL 107(2):1. doi:10.1209/0295-5075/107/28009

[57] Majidi S, Motlagh GH, Bahramian B, Kaffashi B, Nojoumi SA, Haririan I (2013) Rheological evaluation of wet masses for the preparation of pharmaceutical pellets by capillary and rotational rheometers. Pharm Dev Technol 18(1):112–120. doi:10.3109/10837450.2011.640687

[58] Mackaplow MB, Rosen LA, Michaels JN (2000) Effect of primary particle size on granule growth and endpoint determination in high-shear wet granulation. Powder Technol 108(1):32–45. doi:10.1016/s0032-5910(99)00203-x

[59] Ho R, Dilworth SE, Williams DR, Heng JYY (2011) Role of surface chemistry and energetics in high shear wet granulation. Ind Eng Chem Res 50(16):9642–9649. doi:10.1021/ie2009263

[60] Parker MD, York P, Rowe RC (1990) Binder-substrate interactions in wet granulation.1. The effect of binder characteristics. Int J Pharm 64(2–3):207–216. doi:10.1016/0378-5173(90)90270-e

[61] Pantoya ML, Granier JJ (2005) Combustion behavior of highly energetic thermites: nano versus micron composites. Propellants Explos Pyrotech 30(1):53–62

[62] Sharma V, Jaishankar A, Wang Y-C, McKinley GH (2011) Rheology of globular proteins: apparent yield stress, high shear rate viscosity and interfacial viscoelasticity of bovine serum albumin solutions. Soft Matter 7(11):5150–5160. doi:10.1039/C0SM01312A

[63] Plazek DJ, Chelko AJ (1977) Temperature dependence of the steady state recoverable compliance of amorphous polymers. Polymer 18(1):15–18

[64] Shah RD, Kabadi M, Pope DG, Augsburger LL (1995) Physicomechanical characterization of the extrusion–spheronization process.2. Rheological determinants for successful extrusion and spheronization. Pharm Res 12(4):496–507. doi:10.1023/a:1016237509740

[65] Soh JLP, Liew CV, Heng PWS (2006) Torque rheological parameters to predict pellet quality in extrusion–spheronization. Int J Pharm 315(1–2):99–109. doi:10.1016/j.ijpharm.2006.02.023

[66] Mascia S, Patel MJ, Rough SL, Martin PJ, Wilson DI (2006) Liquid phase migration in the extrusion and squeezing of microcrystalline cellulose pastes. Eur J Pharm Sci 29(1):22–34. doi:10.1016/j.ejps.2006.04.011